Available online at www.sciencedirect.com
ScienceDirect
International Journal of Heat and Mass Transfer 51 (2008) 640–649
International Journal of HEAT and MASS TRANSFER
www.elsevier.com/locate/ijhmt

A quantitative analysis on the thermal properties of phosphate buffered saline with glycerol at subzero temperatures

Jeung Hwan Choi [a], John C. Bischof [a,b,c,*]

[a] Department of Mechanical Engineering, University of Minnesota, 111 Church Street SE, Minneapolis, MN 55455, USA
[b] Department of Biomedical Engineering, University of Minnesota, Minneapolis, MN 55455, USA
[c] Department of Urologic Surgery, University of Minnesota, Minneapolis, MN 55455, USA

Received 21 August 2006; received in revised form 29 April 2007
Available online 13 July 2007

Abstract

This study reports the first comprehensive data on the effects of glycerol, a widely used cryoprotective agent (CPA), on the thermal properties of Phosphate Buffered Saline at subzero and cryogenic ($\leqslant -40$ °C) temperatures. A Differential Scanning Calorimeter was used to measure specific and latent heats. Thermal conductivity was determined using a thermistor probe technique. Results differed significantly from known water (ice) or glycerol values, and a simple weight averaging method between water and glycerol was found to overpredict thermal conductivity below −100 °C due to glass formation. This indicates the need for these newly measured thermal properties of CPA solutions particularly below −100 °C.

Keywords: Thermal property; Subzero; Phosphate buffered saline; Glycerol

1. Introduction

Cryobiological applications including cryosurgery or cryopreservation benefit from heat transfer predictions and numerical modeling. The accuracy of the models depends on numerous factors including a correct understanding of the phase change phenomena and knowledge of thermal properties. Valvano [1] measured tissue thermal properties in the temperature range of 3–45 °C. The thermal properties of many foods have been summarized in the ASHRAE Handbook of Refrigeration [2] and provides data between −40 and +149 °C. Fennema [3] et al. also provide thermal properties of many foods down to −40 °C. Bowman et al. [4] tabulated the thermal properties of a large variety of biological materials in the unfrozen range and also provided values of a few materials such as bovine and porcine meat as well as plasma in the subzero range down to −100 °C. Bald and Fraser [5] reviewed the available data on thermophysical properties for various substances and compared them with those for water and ice. Cryoprotective agents are expected to affect the thermal properties of a solution. However, there is a lack of experimental data on the effect of CPA's on thermal properties of physiological solutions in the subzero domain (especially below −40 °C). Therefore, models rely on estimated values based often upon thermal properties of water and ice [6–8] or weight averaged values from known materials [2].

Cooper and Trezek [9] measured the thermal conductivity of various organs by measuring the temperature decay resulting from a step temperature change of a thermocouple probe (copper cylinder with constantan and copper leads) placed inside in vitro and in vivo biomaterials originally at different temperatures. Balasubramaniam and Bowman [10] employed a transient self-heated thermistor technique

* Corresponding author. Address: Department of Mechanical Engineering, University of Minnesota, 111 Church Street SE, Minneapolis, MN 55455, USA. Tel.: +1 612 625 5513; fax: +1 612 625 4344.
E-mail address: bischof@umn.edu (J.C. Bischof).

0017-9310/$ - see front matter © 2007 Elsevier Ltd. All rights reserved.
doi:10.1016/j.ijheatmasstransfer.2007.04.041

Nomenclature

c_p	specific heat, J/kg °C	T	temperature, °C
c_p^*	effective specific heat, J/kg °C	T_i	initial temperature of probe/sample, °C
$c_{p,l}$	specific heat of sample in the liquid phase, J/kg °C	T_g	observed glass transition temperature, °C
$c_{p,s}$	specific heat of sample in the solid phase determined in the complete solid temperature range and also extrapolated into the mushy (phase change) region, J/kg °C	T_g'	glass transition temperature of maximally freeze-concentrated solution, °C
		T_0	temperature at probe center, °C
		T_1	lower temperature point of mushy (phase change) zone, °C
HR	heat absorption ratio of ice melting, $HR(T_1) = 0$, $HR(T_2) = 1$	T_2	upper temperature point of mushy (phase change) zone, °C
k	thermal conductivity, W/m °C	t	elapsed time, s
n	number of experiments/measurements	t_p	duration of pulsed energy, s
P	electrical power input, W	ρ	density, kg/m^3

to measure the thermal conductivity and diffusivity of biological solutions and materials at room temperature. The accuracy of thermal conductivity measurements was reported to be within 1.5%. Subsequent measurements employing the self-heated thermistor technique were performed at physiological temperatures [11] and subzero temperatures down to −70 °C [12] for solutions (perfusates with or without glycerol) and tissues (rabbit kidney). These studies have shown a significant reduction in thermal conductivity due to the addition of glycerol. Further measurement techniques have been developed and reviewed by Chato [13] and Valvano [14]. Recently, Zhang et al. utilized heat probes to measure the thermal conductivity of representative CPA solutions and rabbit organs to −40 °C [15,16]. Finally, one technique involves the utilization of a differential scanning calorimeter (DSC) which has the advantage of requiring small samples [17–19]. However, the technique requires the accurate determination of the sample dimensions as well as reference calibrations and few results seem to have been reported related to biological systems.

The latent heat values of biologically relevant solutions and materials are known to differ from that of pure water (335 J/g). Fennema et al. [3] summarized the latent heats for various foods, and found them to be less than that of water. They correlated the magnitude of the latent heat with the content of water in foods, in which a larger latent heat is associated with more water. Boutron et al. [20–22] measured the latent heat of water/ice phase change in solutions with cryoprotective agents including water–1,2-propanediol, water–glycerol–ethylene glycol, and water–glycerol–ethanol. Devireddy et al. [23] measured the latent heat release of various aqueous solutions above −40 °C in the absence of a eutectic phase change during freezing with a DSC. They reported that the latent heat during water/ice phase change does not correlate with the water content. Han et al. investigated the crystal and eutectic morphology of the phase change to −40 °C and below and the corresponding latent heat release during thawing of several aqueous solutions using both a cryomicroscope and a DSC [24,25]. They found that the latent heats including both water/ice and eutectic phase change do not correlate with the water content, but correlate with the amounts of water and solute that participate in either of the phase changes (i.e. water/ice or eutectic), respectively.

Available specific heat data are relatively limited compared with the availability of thermal conductivity data, and are usually approximated to a weight averaged value of components in a biological system [13]. Specific heats of foods above and below the initial freezing point are tabulated in [2]. The observed specific heats of various foods which include the latent heat are summarized in [3] down to −40 °C and values of some tissue types are presented in [5,9] for temperatures above zero.

This paper aims to address the lack of available information on the effect of CPAs on thermal properties of physiological solutions (especially below −40 °C). Using the DSC and a transient thermistor technique, we show that glycerol affects the latent heat of ice melting, specific heat, and thermal conductivity of isotonic Phosphate Buffered Saline (1×PBS, D-PBS, Life Technology) at subzero temperatures.

2. Materials and methods

2.1. Preparation of solutions

Phosphate buffered saline (Invitrogen Life Technology, D-PBS, Carlsbad, CA) was prepared as an isotonic (1×) physiological solution, and glycerol ($C_3H_8O_3$, molecular weight = 92.1, Sigma–Aldrich, St. Louis, MO) was added to give final concentrations of 1, 2, and 6 M glycerol in PBS.

2.2. Differential scanning calorimetry

A power-compensation type differential scanning calorimeter (Perkin–Elmer, DSC-Pyris 1, Shelton, CT) was used

to observe thermal events during cooling and heating of the solutions. The temperature scale of the DSC was calibrated using two transitional temperatures of cyclohexane (−85.8 °C and 6.4 °C), and the heat flow scale was calibrated against the heat of fusion of pure water (335 J/g) during thawing at 5 °C/min. Subsequent measurements after calibration were conducted using 6–9 mg of each solution in a crimped aluminum sample pan. The samples were prenucleated by supercooling and then reheated to their ice melting temperature. At this temperature, the samples were held for 3 min so that only small amounts of ice were present as nuclei. After the prenucleation step, the samples were cooled to −150 °C and warmed up to 25 °C at 5 °C/min. The resulting thermograms of each freeze–thaw procedure were analyzed to determine latent heat, phase change temperature and specific heat values. Specific heat measurements were performed in regions where no phase change occurred in order to exclude latent heat reactions from being included in specific heat calculations. An extrapolation method explained later was used to determine specific heat within the phase change region. All the specific and latent heat data presented were measured during thawing, which more closely approximates thermodynamic equilibrium conditions [26]. The reported results are an average of 3 measurements per type of sample.

As previously mentioned, all measurements of thermal properties employed a prenucleating step in order to remove supercooling effects in the results obtained. The cooling and heating of the samples at relatively slow rates (5 °C/min) allows us to consider the system as undergoing stepwise quasi-equilibrium changes and has been used previously by others in determining phase diagrams of similar materials [27]. It was assumed that the prenucleation steps would allow sufficient time for crystals to fully develop during the cooling step which would be necessary in interpreting the results as being as close to an equilibrium state as possible. This assumption is reinforced by the fact that no form of devitrification was observed during the heating steps for all of the solutions studied. It should be noted that the methods employed (prenucleated and slow heat–thaw rates) in measuring the thermal properties may not correlate directly with specific cryobiological applications (i.e. cryopreservation) which employ fast freeze and especially thaw rates. The application of faster rates may cause a deviation in thermal properties from the results obtained here, largely due to the difference in crystallization temperatures, crystal growth rates, and the amount of crystals formed at a given temperature [28]. Therefore, while the current study provides new and important data, further studies of non-equilibrium conditions may still be necessary in the future.

2.3. Cryomicroscopy

A light microscope (Olympus, BX50, Melville, NY) was set up with a liquid nitrogen cooled cryostage (Linkam, BCS196, TMS93 & LNP, Surrey, UK) in order to observe phase change characteristics during cooling and heating of the samples. The temperature scanning protocol was identical with the DSC procedure of each sample in order to assure comparable results. Images from the cryomicroscope were recorded with a VCR using a CCD camera (Olympus, OLY-200, Melville, NY) and were processed using a standard personal computer and frame grabber (Integral Technologies, FlashBus MV, Indianapolis, IN). The visual information from the cryomicroscope was then correlated to the quantitative DSC thermogram from the same freeze/thaw protocol.

2.4. Thermal conductivity

An experimental setup based on the pulse decay method (PDM) was employed to measure the thermal conductivity of the samples using a thermistor for both heating and measuring temperature [11]. Thermistor probes were constructed using two types of thermistors (Thermometrics, Edison, NJ) in order to obtain relatively accurate results in the desired temperature range (Model type P60BA102K: −10 to − 80 °C , type CTP60BE105K: −80 to − 150 °C.) The probes are composed of a spherical thermistor component with an outer diameter of 1.5 mm and a trailing cylindrical tail with a slightly smaller diameter and a height of 4.9 mm. Leads are exposed at the outer edge of the tail section. All probes were calibrated by submerging them in an ethanol bath with several reference type T thermocouples and then placing them in a cryo freezer (Planer, Kryo10 Series III, Middlesex, UK). Thermistor resistance values were measured with respect to temperature in order to derive electrical resistance vs. temperature calibration curves. The PDM technique evaluates thermal conductivity by measuring the temperature decay of a thermistor which is heated by a known electric power. A schematic diagram of the measurement setup is shown in Fig. 1. Solution samples of 25 mL were placed in 50 mL centrifuge tubes (Corning Incorporated Life Sciences, product # 430290, Lowell, MA) with an outer diameter of 29.1 mm and submerged in an ethanol bath and then placed inside a cryo freezer in order to facilitate ambient temperature stability during measurements. The samples were first cooled to temperatures 20 °C below those of the actual temperatures desired for measurement and then re-warmed to the finial desired temperature (T_i) in order to minimize supercooling effects from affecting the measurements. Cooling and heating rates were determined to be less than 5 °C/min at all times based on temperature readings in the ethanol bath and the sample.

The pulsing and measurement circuit is largely based on the circuitry used by Chen and Holmes and the reader is referred to [11] for further information. The temperature decay of the probe is calculated with respect to time and applied to the 1-D transient point heat source equation [29] in order to solve for the thermal conductivity:

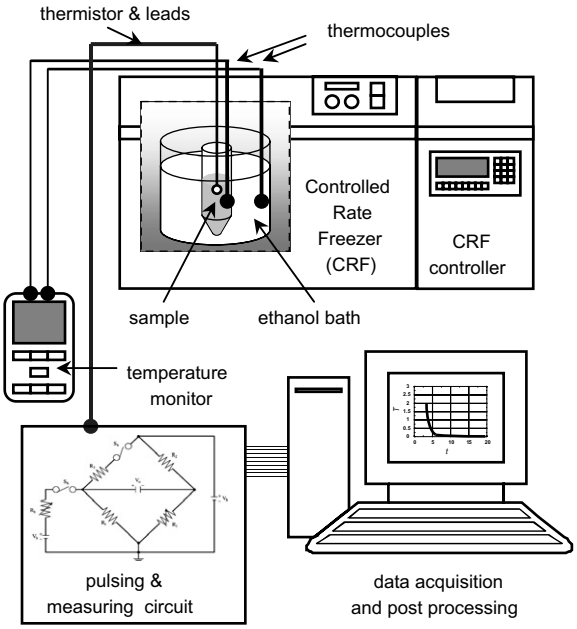

Fig. 1. Schematic diagram of experimental setup for thermal conductivity measurement.

$$T_0(t) - T_i = \frac{P(\rho c_p)^{0.5}}{4(\pi k)^{1.5}}[(t - t_p)^{-0.5} - t^{-0.5}] \quad (1)$$

The electrical input P was varied between 1.2 and 120 mW in order to bring about a temperature rise ($T_o - T_i$) that would not exceed 2 °C during a pulsing duration (t_p) of either 1.5 or 2 s. Thermal conductivity values were determined at time t (between 4.5 and 6 s) when the values stabilized.

3. Results and discussion

Figs. 2a and 2b show representative DSC thermal analyses typical of phase change in solutions. Fig. 2a specifically shows 1×PBS + 6 M glycerol at 5 °C/min without a prenucleation step. It is evident that the sample undergoes a different freeze–thaw event compared with a prenucleated (Fig. 2b) procedure. The crystallization of water (labeled 'a') and the melting of ice (labeled 'd') are clearly evident in these figures. Characteristic changes in heat flow indicative of a glass transition (T_g) are also observed during cooling (labeled 'b') and heating (labeled 'c') near −100 °C for the prenucleated sample while the transition points are shifted to a lower temperature for the sample without prenucleation. This shows that the T_g for the prenucleated sample approaches T_g', the glass transition temperature of a maximally freeze-concentrated solution [30,31]. The events related to a binary or ternary eutectic solidification and melting in the solutions were not readily observed with the DSC, although a small endothermic event during melting (Fig. 2b) near −65 °C was observed. This does not appear to be a melting of the ternary eutectic (∼−80 °C) [27] or the H_2O–glycerol binary system (∼−45 °C) [32].

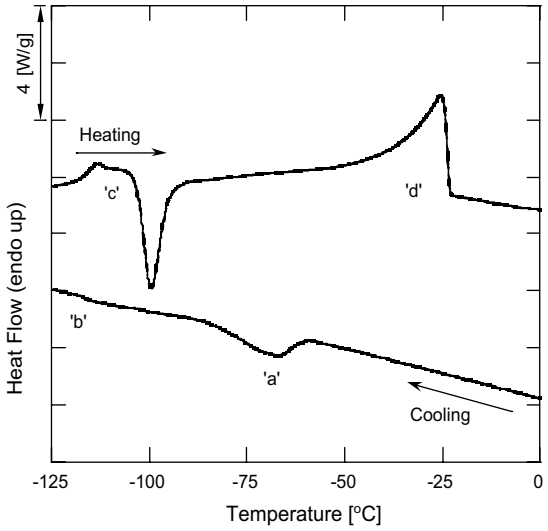

Fig. 2a. DSC thermogram of 1×PBS + 6 M glycerol without prenucleation. Endothermic heat flow into the sample is upward. Lettered events are explained in the text and in figure Fig. 3a.

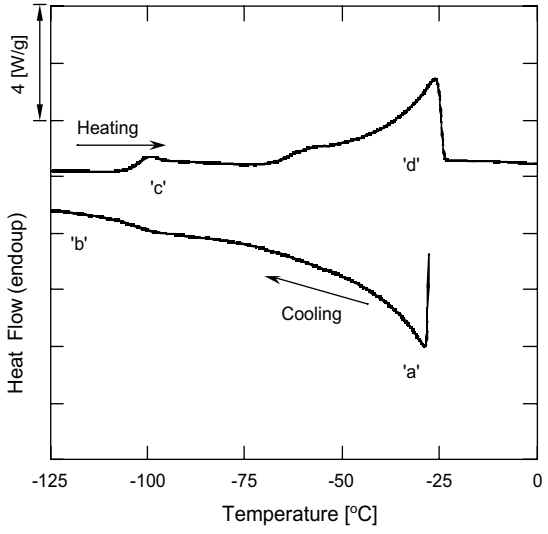

Fig. 2b. DSC thermogram of 1×PBS + 6 M glycerol with prenucleation. Endothermic heat flow into the sample is upward. Lettered events are explained in the text and in figure Fig. 3b.

The existence of a pseudo-binary eutectic in higher concentration PBS solutions without glycerol at −21.2 °C and its effects on the thermal properties has been described previously [33,24].

In order to better understand the enthalpic changes during freezing and thawing of the glycerol–PBS mixtures, cryomicroscopy was used to visualize changes in sample morphology. Figs. 3a and 3b show representative images during cooling and heating of 1×PBS + 6 M glycerol. The locations denoted as 'a–d' in Fig. 2 correspond to the cryomicroscopy results in Fig. 3. When the system was not prenucleated, nucleation and crystal growth occurred near −60 °C (Fig. 3a, label 'a'), while the growth stopped near −100 °C (Fig. 3a, label 'b'). It is assumed

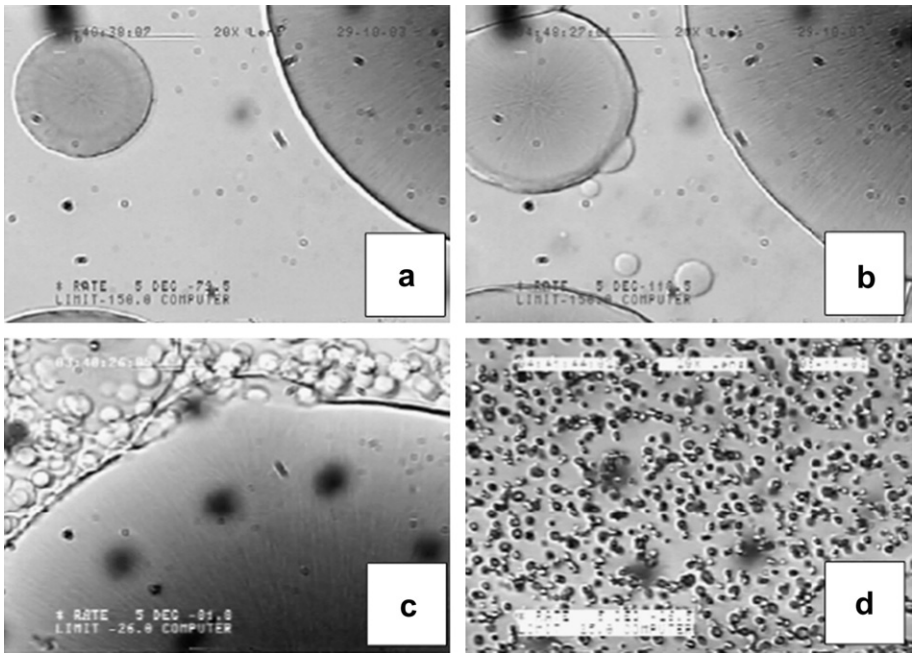

Fig. 3a. Bulk phase change of 1×PBS + 6 M glycerol without prenucleation observed with a cryomicroscope. Scanning rate is 5 °C/min. (a) −73 °C, cooling. (b) −110 °C, cooling. (c) −90 °C, heating. (d) −25 °C, heating. Freeze–thaw methods are explained in the text.

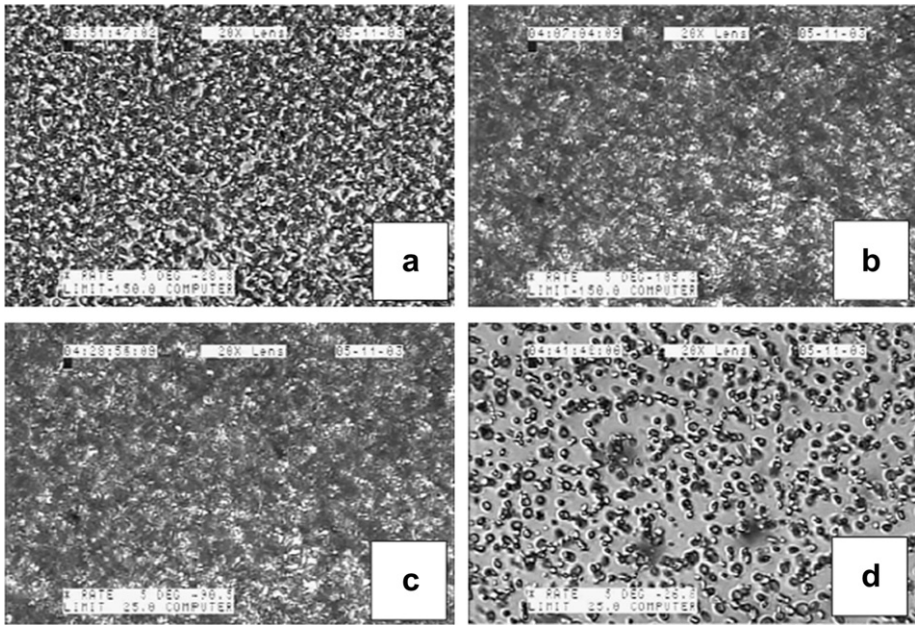

Fig. 3b. Bulk phase change of 1×PBS + 6 M glycerol with prenucleation observed with a cryomicroscope. Scanning rate is 5 °C/min. (a) −28 °C, cooling. (b) −105 °C, cooling. (c) −90 °C, heating. (d) −26 °C, heating. Freeze–thaw methods are explained in the text.

(based on the existence of characteristic glass transition curves defined as increased heat input during both cooling and heating at a temperature point) that the non-frozen fraction vitrified at this point. During reheating, devitrification occurred as evidenced by rapid crystallization of the unfrozen fraction at −100 °C (Fig. 3a, label 'c') as was also observed from phase diagram studies for the NaCl–Glycerol–H_2O system [27]. The sample appeared to remain completely frozen until melting occurred at −25 °C (Fig. 3a, label 'd'). Higher concentrations of glycerol in the samples showed a higher number of ice crystals present, but the size of the crystals was smaller and the propagation speed was reduced. When the system was prenucleated before being cooled to lower temperatures, crystallization occurred at a higher temperature, i.e. without supercooling, (Fig. 3b, label 'a'), and it is assumed that all of the crystal growth occurs during cooling prior to the glass transition (Fig. 3b, label 'b'). This assumption is further reinforced

by the fact that no additional crystal growth was observed during the heating step at temperatures above T_g (Fig. 3b, label 'c') and prior to melting (Fig. 3b, label 'd').

Latent heat and phase change temperature measurements using the DSC are shown in Table 1. The melting points of ice (T_m) for the solutions studied were compared with data in the literature for H_2O–glycerol [32], H_2O–NaCl–glycerol [34,27] and H2O-NaCl [35] as shown in Fig. 4. X_g is defined as the weight ratio of glycerol versus the entire solute weight. T_m data from the current study for PBS + glycerol closely follows the curve corresponding to $X_g = 1$ due to the small amount of solutes present in the system other than glycerol. The latent heats of fusion of the ice component which solidified for the solutions studied were compared with other data available in the literature as shown in Fig. 5, where the latent heat values were normalized with respect to the entire sample weight [20–22,24]. X_c is defined as the weight ratio of the non-NaCl component versus the entire solute weight. It appears that 1×PBS with varying concentrations of glycerol closely follows the $X_c = 1$ curve, but limited data in the lower concentration range of the $X_c = 1$ curve makes it difficult to derive a conclusion.

As can be seen from the latent heat measurement results of Table 1, an increase in glycerol concentration reduces the latent heat during melting. This is due to the fact that the latent heat values are tabulated based on normalization with respect to the total sample weight, and thus reduce in value since there is less ice melting within the system when the glycerol concentration is increased. A better quantification of the latent heat of ice would be possible if one were to employ a normalization method based on dividing the endothermic heat by the amount of H_2O actually participating in the melting of ice [25]. However, this requires knowledge of all other heat absorption/release activities during the freeze–thaw event including the existence of any pseudo-binary or ternary eutectic components. Therefore, the reported latent heat values should be utilized as a "bulk" property in its applications to other analyses.

Specific heat measurements are shown in Fig. 6. The specific heat of H_2O reported by Bald and Fraser [5] is

Table 1
Latent heat and temperature of melting of PBS with glycerol

Solution	Latent heat [J/g]	Melting temperature [°C]
1×PBS	305.9 ± 5.7	−0.5 ± 0.2
1×PBS + 1 M glycerol	238.2 ± 6.2	−1.97 ± 0.6
1×PBS + 2 M glycerol	178.6 ± 1.6	−5.5 ± 0.3
1×PBS + 6 M glycerol	47.1 ± 3.5	−26.3 ± 0.8

DSC scanning rates are 1–5 °C/min. Latent heat values are normalized with respect to entire sample weight. Error values are one standard deviation with $n = 3$.

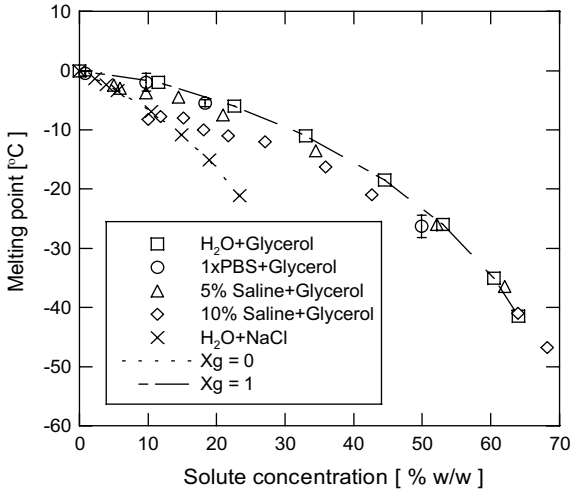

Fig. 4. Melting point of ice for various solutions. Data set (□) from [32], (○) measured from current study with $n = 3$ and error bars indicating standard deviation, (Δ)(◇) from [34,27], (×) from [35]. X_g is the ratio of glycerol versus solute weight.

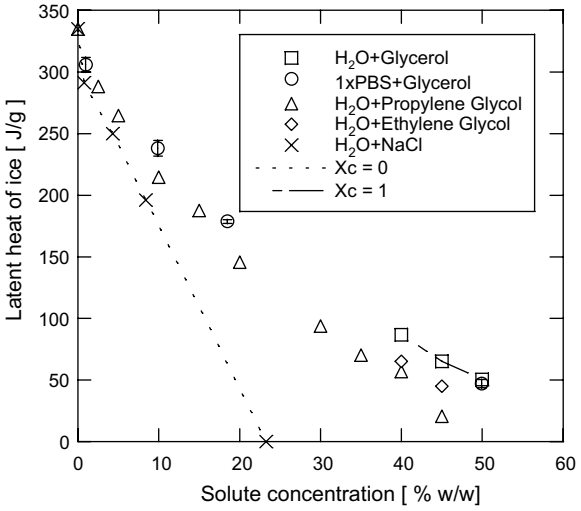

Fig. 5. Latent heat of fusion of ice for various solutions. Data set (×) from [24], (○) measured from current study with $n = 3$ and error bars indicating standard deviation, all others from [20–22]. X_c is the ratio of the non-NaCl component versus the entire solute weight. Latent heat values are normalized with respect to the entire sample weight.

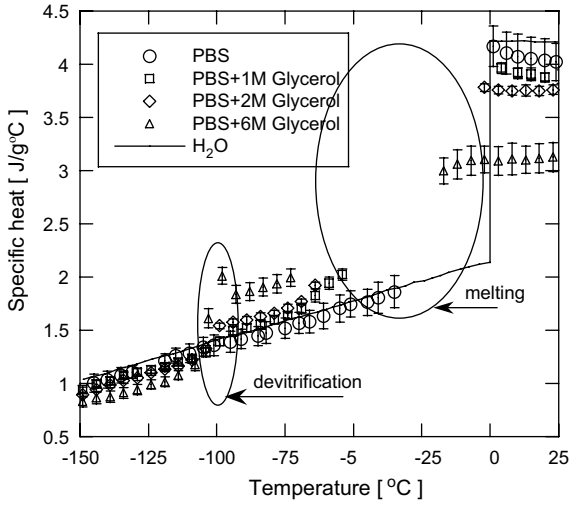

Fig. 6. Specific heat data of 1×PBS + glycerol solutions. All DSC scanning rates are 5 °C/min and $n = 3$. Error bars indicate standard deviation. H_2O values are from [5].

shown for comparison. It is observed that for samples with glycerol being heated from −150 °C, higher glycerol concentrations show a smaller value in specific heat value prior to what appears to be devitrification at around −100 °C [27,22]. Interestingly higher specific heat values are subsequently observed for higher glycerol concentrations in the crystalline state (which is similar with the results from [30]). However, this trend is reversed again during melting, where higher glycerol concentration solutions once again exhibit lower specific heat values. In the absence of available specific heat data at subzero temperatures for biologically relevant solutions it is difficult to make a comparison to the current results. The changes in trends of the observed specific heat values occurring at the glass-to-crystal and crystal-to-liquid temperature points suggest that the specific heat of the various components within the solid have different values and are likely to be ordered as:

c_p : glassy mixture < ice < liquid solution < water

The results for thermal conductivity measurements using the PDM technique are shown in Fig. 7. The thermal conductivity of PBS closely follows that of H_2O but begins to deviate from that of water at temperatures below −65 °C. Glycerol counteracts the increase in thermal conductivity with decreasing temperature that is observed in PBS and water. The drastic increase in thermal conductivity at low temperatures that is observed in water and PBS is less pronounced upon addition of glycerol. At a glycerol concentration of 2 M, the thermal conductivity remains constant between −90 and −150 °C. The thermal conductivity actually appears to slightly drop in the 6 M glycerol sample below the glass transition temperature near −100 °C [27]. In order to better understand the trends of the thermal conductivity values the range of data was extended into the mushy zones of the solutions studied, as shown in Fig. 8. This was done by deriving an effective specific heat value to be used in calculating (Eq. (1)) the thermal conductivity within the mushy zone. The effective specific heats were determined for temperatures between T_1 and T_2 as

$$c_p^*(T) = c_{p,s}(T) + \mathrm{HR}(T) \times [c_{p,l}(T_2) - c_{p,s}(T_2)] \quad (2)$$

The data set was also extended into the complete liquid zone for PBS + 6 M glycerol at around −10 °C. The error bars shown in Fig. 8 indicate the maximum and minimum values which would be derived if we assume the specific heat values to be fully liquid or fully solid, respectively, within the mushy zones. It can be inferred from the results that the thermal conductivity values increase with lower temperatures until the glass formation temperature, after which the rising trend is suppressed in varying degrees depending on the concentration of glycerol (i.e. the amount of glass or amorphous phase present). These results allow us to speculate on the effects of the various components within the sample, where the transition of water into ice would increase thermal conductivity, while the transition of the liquid mixture into an amorphous phase would decrease it. The observation of relatively high thermal conductivity values at −10 °C for the 1 and 2 M glycerol samples can be understood based on two factors; liquid content and viscosity. The existence of a liquid phase in the sample will result in a thermal conductivity measurement higher than expected due to increased heat flux through convection. Therefore the 2 M sample, which has a larger amount of melted ice at −10 °C compared to the 0 or 1 M samples will be more susceptible to an overestimation error. Although liquid content would be highest for the 6 M

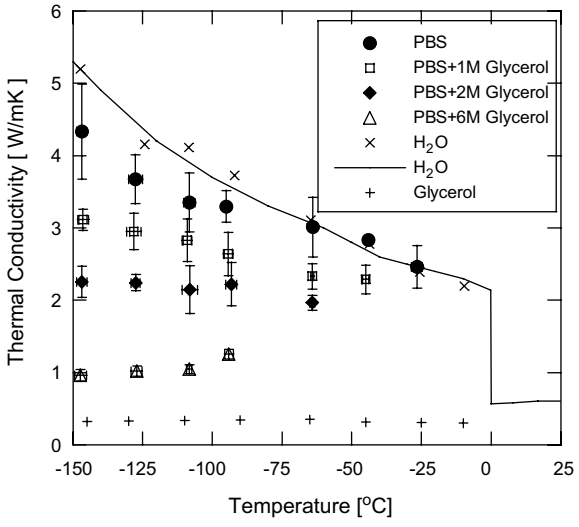

Fig. 7. Thermal conductivity data of 1×PBS + glycerol ($n = 3$ or more). Error bars indicate standard deviation. H_2O values are from [5,42,43], glycerol values are from [36,44].

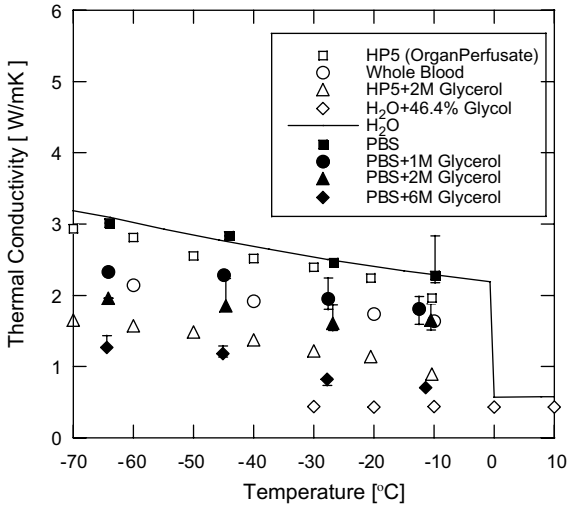

Fig. 8. Extended thermal conductivity data for various solutions including the mushy and liquid zones. Data set (□)(Δ) from [12], (○) from [4], (◇) from [16], (–) from [5], (■)(●)(▲)(♦) measured from current study. Error bars are explained in the text.

sample, the higher viscosity value of the sample would suppress convection effects, and errors would lessen with high concentration samples.

The thermal conductivity data for PBS with glycerol was compared with other data available in the literature as shown in Fig. 8 [4,5,12,16]. The thermal conductivity of PBS is similar to other solutions with high water content, such as HP5 (an organ perfusate). The values for PBS + 1 M glycerol appear to be similar to those for whole blood in the temperature region shown. The values for PBS + 2 M glycerol appear to be similar with those observed for HP5 + 2 M glycerol, with some offset probably due to the difference in solute types and concentration other than glycerol and H_2O within these solutions.

It is evident that the thermal conductivity decreases with increasing glycerol concentrations. The property of the amorphous state seems to be dependent upon temperature as well, based on the observation that the thermal conductivity value continued to decrease with lower temperatures after glass transition for the 6 M glycerol sample. This trend is analogous to that which is observed for thermal conductivity values of pure glycerol [36] which falls with further cooling after glass transition.

In order to see how our measurement results would compare with analytically predicted thermal properties data, the weight-approximation prediction method performed by Rubinsky and Cravalho [37] was graphed along with our results as shown in Fig. 9. The predicted values for the 0.145 M NaCl solution with 1 and 2 M glycerol show a similar trend with the measurement values of the current study for the same glycerol concentrations. However, the predicted values were at times significantly higher (as much as 20%) compared to the measured values. When extended to below −100 °C the predictions also fail to show a drop in thermal conductivity after glass transition as is the case for our measurements. This suggests that when available, accurate modeling should rely on measured thermal properties. The cause of the discrepancy can be due to several factors. Firstly, the weight averaged values shown did not include the contributions of NaCl in the final value of the bulk thermal conductivity. This factor is not expected to be of great importance since the concentration of NaCl is very low. A second factor is that weight averaging adds up the effect of the individual substances acting by themselves, while in reality a combined effect of multiple components dispersed within a system needs to be considered in determining the thermal conductivity [38,39]. A third factor which needs to be considered is the existence of metastable phases in the samples even from relatively slow cooling rates of around 5 °C/min. Due to the high tendency of glycerol to supercool and produce metastable phases the total amount of ice, predicted from a phase diagram, would not completely precipitate in the samples studied [40], and would result in a reduction of the bulk thermal conductivity. Addressing these factors, one would need to formulate a new weight averaging equation, for which the fractions of ice, unfrozen liquid, and glassy phase need to be determined as functions of temperature and cooling or heating rate. The thermal conductivity of the individual components of unfrozen liquid and a glassy phase would have to be known as well.

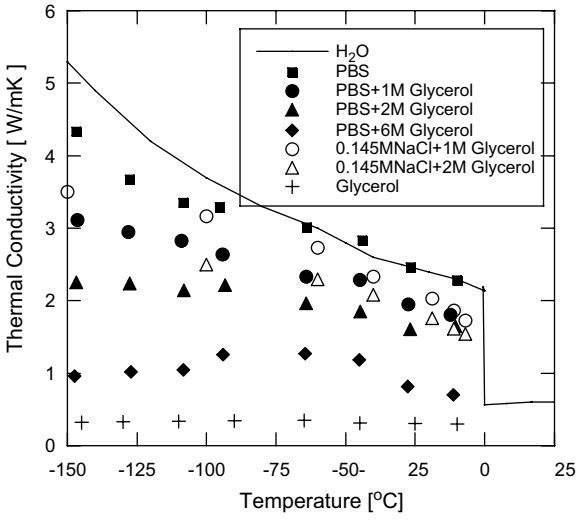

Fig. 9. Comparison of measured data from current study with predictions from Rubinsky and Cravalho (○) (Δ) [37]. H_2O values are from [5,42,43], glycerol values are from [36,44].

4. Measurement uncertainties

Measurement uncertainties for the DSC and pulse decay methods were estimated and where possible tested using a perturbation scheme described below. Instrumental errors were considered zeroth-order uncertainties which originate from the instrument itself and are not due to the changes in the sample measured or the conditions under which the measurements are made. These errors were determined by using calibration standard materials and measuring their thermal characteristics using the same sample for repeated measurements. The standard deviation of this error was ±0.05 °C while it was ±0.7 J/g °C for the latent heat value. Measurement error is defined here as the standard deviation value obtained for a thermal property based on using multiple samples ($n = 3$ or greater) for measurements. Therefore measurement errors would contain higher order uncertainties originating from the use of multiple samples under varying conditions at which measurements are made in addition to zeroth-order uncertainties originating from instrumental errors. The errors reported in Table 1 are measurement errors which exceed instrumental errors due to variations in sample concentrations and/or inconsistencies in preparing and loading the solutions. The measurement errors of specific heat in the subzero range for PBS with 0 M, 1 M, 2 M, and 6 M glycerol (Fig. 6) were ±0.15, ±0.1, ±0.04, and ±0.14 J/g °C, respectively.

While specific heat is a direct DSC measurement, thermal conductivity is based on using multiple measurements and thus error (overall-measured) is estimated using a

perturbation scheme. It is thus an open question whether the reported measurement errors for thermal conductivity (Fig. 7) in turn are influenced by the measurement errors of specific heat and density, stability of the bridge voltage, and reliability of the resistance-to-temperature calibration curve, to name a few. To estimate the importance of each possible error in contributing to overall error an input perturbation scheme was applied to the thermal conductivity Eq. (1). The input values of the DSC-measured specific heat and density (based on [41]) have a maximum expected error of 2.6% and 0.9% error, respectively. The maximum voltage measurement error is 1.6%, and resistance-to-temperature calibration curves will also introduce a maximum error of 1.9%. The combined effects of these errors were calculated to bring about predicted error values which were usually two-thirds of what was determined from actual measurements. The differences are attributed to variations in sample preparation, compositional non-homogeneity of the bulk sample, contact resistance at the thermistor–sample interface, and differences in the radial conduction pathway due to the existence of coated lead connections to the thermistor. As the perturbation method errors are less than the reported (Fig. 7), we use the standard deviation generated from the actual measurements of variables and their conversion to k using Eq. (1).

It is noted that two other factors were originally considered in addition to the above-mentioned factors. There was a possibility that errors would be introduced due to the fact that a point–source relationship was used to determine the thermal conductivity using a finite sized (1.2 mm) probe and also due to the thermal response times associated with the thermistor in transient operation. The former would result in an over-prediction, while the latter would give us an under-prediction. Another series of analyses have shown (Fig. 10) that the effects of these two factors become negligible (less than 0.5%) with a sufficient passage of time (and hence measurements were made 4.5–6 s after pulsing has ceased) when the decay profile for the point and finite sized sources become similar and when the change in temperature per unit time becomes small.

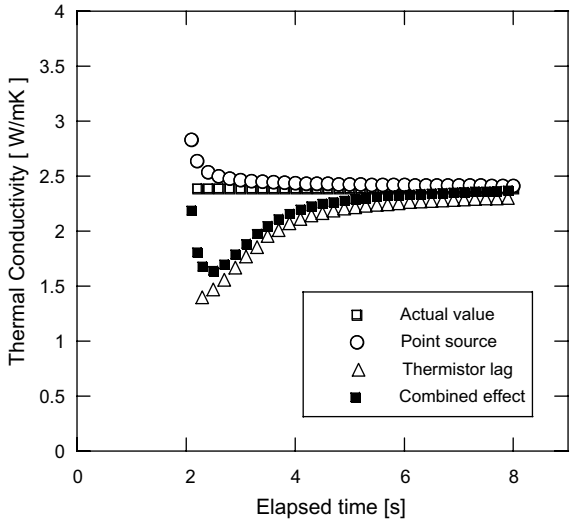

Fig. 10. Thermal conductivity prediction errors due to calculation and operational methods. Shown is the result for a single measurement of the thermal conductivity of ice at −25 °C after a 2 s pulsing event. The actual thermal conductivity value (□) should remain constant regardless of the time at which calculations are made. The point–source equation used for calculations for the finite-sized probe would bring about an overestimation which is pronounced at early times (○). Thermal lag associated with the probe would produce a large underestimation at early times (Δ). The combined effect of these errors would produce a prediction as shown in (■) which become negligible after a sufficient passage of time (4.5–6 s).

5. Conclusion

Current results indicate that there exists a substantial difference in subzero thermal property values between H_2O and PBS with glycerol. Therefore it is largely inappropriate to assume thermal properties of H_2O in an analysis involving cryobiologically relevant solutions especially at lower subzero temperatures. In summary, the reported values for latent heat and specific heat as well as the determined values for thermal conductivity can be used in physics-based numerical modeling such as finite volume, or finite element, based numerical models. In some cases, however, time-dependent properties, due to the competition between crystalline and amorphous (i.e. non-equilibrium) phases, would have to be used through empirical relations which were not the focus of this study. Further work will focus on translating these methods to measurements within cryobiologically relevant tissue systems with or without CPA loading.

Acknowledgements

This work was supported by the United States National Science Foundation (NSF) under Grant No. CTS 0313934. The authors thank Dr. Willem F. Wolkers for a careful read of the manuscript.

References

[1] K.R. Diller, J.W. Valvano, J.A. Pearce, Bioheat transfer, in: F. Kreith (Ed.), The CRC Handbook of Thermal Engineering, CRC Press, Boca Raton, 1999 (Sec. 4.4).
[2] ASHRAE, Thermal properties of foods, in: M.S. Owen (Ed.), ASHRAE Handbook – Refrigeration, ASHRAE, New York, 2002 (Chapter 8).
[3] O.R. Fennema, W.D. Powrie, E.H. Marth, Low-temperature Preservation of Foods and Living Matter, Marcel Dekker Inc., New York, 1973.
[4] H.F. Bowman, E.G. Cravalho, M. Woods, Theory, measurement and application of thermal properties of biomaterials, Annu. Rev. Biophys. Bioeng. 4 (1975) 43–82.
[5] W.B. Bald, J. Fraser, Cryogenic surgery, Rep. Prog. Phys. 45 (1982) 1381–1434.
[6] J. Klinger, Thermal conductivity of ice single crystals at low temperatures, in: symposium on the Physics and Chemistry of Ice, Royal Society of Canada, 1973, pp. 114–116.
[7] T. Ashworth, Measurement of the thermal properties of ice, in: Proceedings of the Fourth International Cryogenic Engineering Conference, IPC Science and Technology Press Ltd., 1972.

[8] P.V. Hobbs, Ice Physics, Clarendon Press, Oxford, 1974.
[9] T.E. Cooper, G.J. Trezek, A probe technique for determining the thermal conductivity of tissue, J. Heat Transfer (1972) 133–140.
[10] T.A. Balasubramaniam, H.F. Bowman, Thermal conductivity and thermal diffusivity of biomaterials: a simultaneous measurement technique, J. Biomech. Eng. 99K (1977) 148–154.
[11] M.M. Chen, K.R. Holmes, V. Rupinskas, Pulse-decay method for measuring the thermal conductivity of living tissues, J. Biomech. Eng. 103 (1981) 253–260.
[12] X. Bai, D.E. Pegg, Thermal property measurements on biological materials at subzero temperatures, J. Biomech. Eng. 113 (1991) 423–429.
[13] J.C. Chato, Measurement of thermal properties of biological materials, in: A. Shitzer, R.C. Eberhart (Eds.), Heat Transfer in Medicine and Biology, Plenum Press, New York, 1985 (Chapter 8).
[14] J.W. Valvano, Low temperature tissue thermal properties, in: J.J. McGrath, K.R. Diller (Eds.), Low Temperature Biotechnology: Emerging Applications and Engineering Contributions, vol. 10, ASME, New York, 1988.
[15] A. Zhang, S. Cheng, L. He, D. Luo, D. Gao, Determination of thermal conductivity of cryoprotectant solutions and cell suspensions, Cell Preserv. Technol. 2 (2004) 157–162.
[16] H. Zhang, S. Cheng, L. He, A. Zhang, Y. Zheng, D. Gao, Determination of thermal conductivity of biomaterials in the temperature range 233–313 K using a tiny detector made of a self-heated thermistor, Cell Preserv. Technol. 1 (2002) 141–147.
[17] J. Chiu, P.G. Fair, Determination of thermal conductivity by differential scanning calorimetry, Thermochim. Acta 34 (1979) 267–273.
[18] Y.P. Khanna, T.J. Taylor, G. Chomyn, A new differential scanning calorimetry based approach for the estimation of thermal conductivity of polymer solids and melts, Polym. Eng. Sci. 28 (1988) 1034–1041.
[19] M.Y. Keating, C.S. McLaren, Thermal conductivity of polymer melts, Thermochim. Acta 166 (1990) 69–76.
[20] P. Boutron, A. Kaufmann, Stability of the amorphous state in the system water–1,2-propanediol, Cryobiology 16 (1979) 557–568.
[21] P. Boutron, A. Kaufmann, Stability of the amorphous state in the system water–glycerol–ethylene glycol, Cryobiology 16 (1979) 83–89.
[22] P. Boutron, A. Kaufmann, N.V. Dang, Maximum in the stability of the amorphous state in the system water–glycerol–ethanol, Cryobiology 16 (1979) 372–389.
[23] R.V. Devireddy, P.H. Leo, J.S. Lowengrub, J.C. Bischof, Measurement and numerical analysis of freezing in solutions enclosed in a small container, Int. J. Heat Mass Transfer 45 (2002) 1915–1931.
[24] B. Han, J.C. Bischof, Thermodynamic nonequilibrium phase change behavior and thermal properties of biological solutions for cryobiology applications, J. Biomech. Eng. 126 (2004) 196–203.
[25] B. Han, J.H. Choi, J.A. Dantzig, J.C. Bischof, A quantitative analysis on latent heat of an aqueous binary mixture, Cryobiology 32 (2006) 146–151.
[26] G. Hohne, W. Hemminger, H.J. Flammersheim, Differential Scanning Calorimetry: An Introduction for Practitioners, Springer, New York, 1996.
[27] M.L. Shepard, C.S. Goldston, F.H. Cocks, The H_2O–NaCl–glycerol phase diagram and its application in cryobiology, Cryobiology 13 (1976) 9–23.
[28] J.M. Hey, D.R. MacFarlane, Crystallization of ice in aqueous solutions of glycerol and dimethyl sulfoxide 2: ice crystal growth kinetics, Cryobiology 37 (1998) 119–130.
[29] H. Carslaw, J. Jaeger, Conduction of Heat in Solids, Clarendon Press, Oxford, 1959.
[30] L. Her, S.L. Nail, Measurement of glass transition temperatures of freeze-concentrated solutes by differential scanning calorimetry, Pharmaceut. Res. 11 (1994) 54–59.
[31] G.J. Morris, M. Goodrich, E. Acton, F. Fonseca, The high viscosity encountered during freezing in glycerol solutions: effects on cryopreservation, Cryobiology 52 (2006) 323–334.
[32] L.B. Lane, Freezing points of glycerol and its aqueous solutions, Ind. Eng. Chem. 17 (1925) 924.
[33] B. Han, J.C. Bischof, Effect of thermal properties on heat transfer in cryopreservation and cryosurgery, in: Proceedings of the ASME 2002 International Mechanical Engineering Congress and Exposition, IMECE2002-33664, ASME, 2002.
[34] D.E. Pegg, Simple equations for obtaining melting points and eutectic temperatures for the ternary system glycerol/sodium chloride/water, Cryo-Letters 4 (1983) 259–268.
[35] R.E. Hall, M.S. Sherrill, International Critical Tables of Numerical Data, Physics, Chemistry and Technology, vol. 4, McGraw-Hill, New York, 1928.
[36] D.G. Cahill, R.O. Pohl, Thermal conductivity of amorphous solids above the plateau, Phys. Rev. B 35 (1987) 4067–4073.
[37] B. Rubinsky, E.G. Cravalho, An analytical method to evaluate cooling rates during cryopreservation protocols for organs, Cryobiology 21 (1984) 303–320.
[38] R.B. Bird, W.E. Stewart, E.N. Lightfoot, Transport Phenomena, second ed., Wiley, New York, 2002.
[39] M. Jakob, Heat Transfer, vol. 1, John Wiley & Sons, New York, 1949.
[40] P. Boutron, Comparison with the theory of kinetics and extent of ice crystallization and of the glass-forming tendency in aqueous cryoprotective solutions, Cryobiology 23 (1986) 88–102.
[41] J.C. Bischof, B. Mahr, J.H. Choi, M. Behling, D. Mewes, Use of X-ray tomography to map crystalline and amorphous phases in frozen biomaterials, Ann. Biomed. Eng. 35 (2007) 292–304.
[42] CRC, Properties of ice and supercooled water, in: Handbook of Chemistry and Physics, 87 ed., Taylor and Francis, Boca Raton, 2006.
[43] G.A. Slack, Thermal conductivity of ice, Phys. Rev. B 22 (1980) 3065–3071.
[44] N.O. Birge, Specific-heat spectroscopy of glycerol and propylene glycol near the glass transition, Phys. Rev. B 34 (1986) 1631–1642.